Molecular Therapy
Methods & Clinical Development
Original Article

Small Alphaherpesvirus Latency-Associated Promoters Drive Efficient and Long-Term Transgene Expression in the CNS

Carola J. Maturana,[1] Jessica L. Verpeut,[1] Thomas J. Pisano,[1] Zahra M. Dhanerawala,[1] Andrew Esteves,[2] Lynn W. Enquist,[2] and Esteban A. Engel[1]

[1]Princeton Neuroscience Institute, Princeton University, Princeton, NJ 08544, USA; [2]Department of Molecular Biology, Princeton University, Princeton, NJ 08544, USA

Recombinant adeno-associated viruses (rAAVs) are used as gene therapy vectors to treat central nervous system (CNS) diseases. Despite their safety and broad tropism, important issues need to be corrected such as the limited payload capacity and the lack of small gene promoters providing long-term, pan-neuronal transgene expression in the CNS. Commonly used gene promoters are relatively large and can be repressed a few months after CNS transduction, risking the long-term performance of single-dose gene therapy applications. We used a whole-CNS screening approach based on systemic delivery of AAV-PHP.eB, iDisco+ tissue-clearing and light-sheet microscopy to identify three small latency-associated promoters (LAPs) from the herpesvirus pseudorabies virus (PRV). These promoters are LAP1 (404 bp), LAP2 (498 bp), and LAP1_2 (880 bp). They drive chronic transcription of the virus-encoded latency-associated transcript (LAT) during productive and latent phases of PRV infection. We observed stable, pan-neuronal transgene transcription and translation from AAV-LAPs in the CNS for 6 months post AAV transduction. In several CNS areas, the number of cells expressing the transgene was higher for LAP2 than the large conventional EF1α promoter (1,264 bp). Our data suggest that the LAPs are suitable candidates for viral vector-based CNS gene therapies requiring chronic transgene expression after one-time viral-vector administration.

INTRODUCTION

Recent improvements made to recombinant adeno-associated viruses (AAVs), including capsid engineering and novel gene promoters, have substantially increased downstream gene therapy applications.[1,2] AAV vectors are widely used in neuroscience and clinical applications given their safety, serotype-dependent broad tropism, and transduction efficiency.[3,4] AAV-9 synthetic variant PHP.eB,[5] with an enhanced ability to permeate the mouse blood-brain barrier (BBB) and broadly transduce central nervous system (CNS) neurons both in the brain and spinal cord after peripheral vascular administration, is one example of recent capsid improvements.[6] A major limitation of recombinant AAVs is their small capsid with a limited payload capacity of only ~4.9 kb.[7] Accordingly, the discovery of short promoter sequences able to sustain strong and long-lived transcription is paramount to expand the transgene payload and achieve chronic therapeutic effect with one viral dose.

Several strong promoters such as neuron-specific enolase (NSE; 1,800 bp),[8,9] calcium/calmodulin-dependent protein kinase II alpha (CaMKIIa; 1,300 bp),[10] and human elongation factor 1 alpha (EF1α; 1,264 bp)[10,11] have been used in systemic AAV delivery.[4] However, the considerable size of these promoter sequences limits the use of large therapeutic transgenes or multiple small transgenes. Moreover, short promoters such as the human cytomegalovirus immediate-early enhancer and promoter (CMV; 600 bp)[12] or truncated versions of the human synapsin promoter (hSyn; 468 bp)[13] are considerably weaker to drive gene transcription and expression, and in some cases, are completely repressed or inactivated only weeks after delivery.[11,13–16] Similarly, small ubiquitous promoters such as beta glucuronidase (GUSB; 378 bp)[17] or ubiquitin C (UBC; 403 bp)[11,18] have shown weak transcription levels.

In this study, we describe and validate three alphaherpesvirus latency-associated promoters (LAPs), called LAP1 (498 bp), LAP2 (404 bp), and LAP 1_2 (880 bp), obtained from the genome of the herpesvirus pseudorabies virus (PRV). The Alphaherpesvirinae subfamily of the family Herpesviridae includes bovine herpes virus-1 (BHV-1), varicella-zoster virus (VZV), herpes simplex virus (HSV), and PRV. These viruses share genome organization and establish latent infections in sensory ganglia of different mammalian hosts.[19,20] Several studies have established the role of LAPs in promoting long-term expression, since LAPs can chronically drive transcription of the latency-associated transcript (LAT), even under highly repressible and adverse conditions.[21–25] The LAP region of PRV encompasses two tandem independent promoters, LAP1 and LAP2.[23,26–28] PRV LAP1 contains two GC boxes and three CAAT boxes upstream of the first TATA box. PRV LAP2 contains two GC boxes before the

Received 13 January 2020; accepted 6 April 2020;
https://doi.org/10.1016/j.omtm.2020.04.004.

Correspondence: Esteban A. Engel, Princeton Neuroscience Institute, Princeton University, Princeton, NJ 08544, USA.
E-mail: eengel@princeton.edu

second TATA box.[23,27,29] It has been proposed that the binding of different transcription factors (TFs) to consensus promoter elements present in LAPs may facilitate escape from nucleosome silencing during latent infection.[28,30,31] In transgenic mouse lines, PRV LAP-mediated transcription is neuron-specific in the absence of PRV infection.[32] However, in transient expression assays, PRV LAP1 and LAP2 promoted transcription both in cultured neuronal as well as non-neuronal cells.[26,29] Furthermore, the activity of tandem LAP1 and LAP2 sequences is significantly increased compared to LAP1 or LAP2 alone.[26]

In the present study, we tested PRV LAPs in AAV vectors for *in vivo* whole-CNS transduction. We found that PRV LAP1, LAP2, and tandem LAP1_2 promoters are suitable for systemic, less invasive, pan-neuronal gene delivery applications that may require stable, chronic transgene expression after a single administration.

RESULTS

Small PRV LAP Variants Can Drive Transgene Expression in Neurons Independently of Herpesvirus Infection

The PRV LAP region includes at least two promoter regions defined here as LAP1 and LAP2 (Figure 1A). In the PRV genome, LAP1 and LAP2 are present in tandem as PRV LAP1_2. These sequences alone or combined are capable of efficient expression of reporter transgenes in primary sympathetic neurons when used in AAV vectors without PRV infection (Figures 1C and 1D). We analyzed the LAP nucleotide sequences to identify putative regulatory elements using JASPAR,[33] RSAT,[34] and CTCFBSDB 2.0[35] software. We identified three cyclic AMP response element-binding proteins (CREBs) located upstream of the LAP1 TATA box and one upstream of the LAP2 TATA box. Moreover, two CTCF motifs (CCCTC-binding factor) were detected upstream of the LAP1 TATA box and one downstream of the LAP2 TATA box. We identified downstream promoter elements (DPEs) in LAP2, including CG boxes and four signal transducer and activator of transcription 1 (STAT1) sites. Additionally, there were lineage-determining TFs,[36] such as SRY-box 10 (SOX10) and oligodendrocyte TF2 (Olig2), upstream of the LAP1 TATA box and LAP2 TATA box, respectively (Figure 1A).

Four AAV recombinants were packaged into serotype PHP.eB capsids by standard methods, each containing LAP1 (498 bp), LAP2 (404 bp), and LAP 1_2 (880 bp) promoter sequences. We used the ubiquitous EF1α promoter (1,264 bp) as a positive transgene expression control. All four AAV recombinants expressed the fluorescent reporter mCherry (Figure 1B). To verify the *in vitro* performance of each promoter, we transduced rat primary superior cervical ganglion (SCG) neuronal cultures with 3×10^{11} viral genomes (vg) of each AAV and quantified the relative fluorescence intensity (RFI) arbitrary units (A.U.) of mCherry during a 90-day period. For neurons transduced with AAV-LAP1, mCherry expression increased abruptly at 11 days post-infection (dpi) (6.42×10^4 RFI) but to a lower level when compared with AAV-LAP2, AAV-LAP1_2, and AAV-EF1α. AAV-LAP2 and AAV-EF1α expression increased ~125-fold more at 17 dpi (8.70×10^6 and 8.01×10^6 RFI, respectively) (Figure 1C). The highest level of expression was at 28 dpi with LAP1 (2.9×10^5 RFI), LAP2 (1.36×10^7 RFI), LAP1_2 (4.36×10^6 RFI), and EF1α (1.40×10^7 RFI) (Figures 1C and 1D). LAP2 and EF1α achieved the highest mCherry RFI (LAP2 = EF1α > LAP1_2 > LAP1). Between 38 and 90 dpi, all four AAV recombinants showed a subtle but sustained RFI decrease (Figure 1C), most likely due to the senescence of primary SCG neurons after more than 100 days in culture. Importantly, all three AAV-LAP recombinants showed mCherry transcription in primary neurons for 90 days in the context of AAV transduction and in the absence of PRV infection.

Whole-CNS Screening Reveals Pan-neuronal AAV-LAP Transgene Expression after 6 Months

We used AAV serotype PHP.eB for our promoter screening assay given the enhanced capacity to cross the BBB and transduce C57BL/6 mice CNS after systemic, intravascular delivery.[5] AAV-LAP1-mCherry, AAV-LAP2-mCherry, AAV-LAP1_2-mCherry, and AAV-EF1α-mCherry were delivered by unilateral retro-orbital venous sinus injection of 4×10^{11} vg/mouse). The brains and spinal cords were harvested 30 and 190 dpi, as described in Figure 2A, to quantify mCherry transcription and translation. LAP-mCherry expression in the whole intact brain was determined by tissue clearing and immunostaining with iDISCO+ (immunolabeling-enabled three-dimensional imaging of solvent-cleared organs) and visualized by light-sheet microscopy and volumetric registration (Videos S1, S2, S3, and S4).[37,38] All four gene promoters showed stable mCherry expression at both 30 and 190 dpi. The density (number of mCherry-positive cells per mm^3 of brain tissue) of LAP2 was higher than that of LAP1 and LAP1_2, and it had no significant differences from EF1α ($p < 0.05$) in different areas of the cortex, including primary motor, secondary motor, primary somatosensory, and supplemental somatosensory cortex (Figures 2B–2E, respectively), hippocampal formation (Figure 2G), pallidum (Figure 2I), hypothalamus (Figure 2K), and olfactory areas (Figure 2P). In cerebellum, LAP2 showed significantly higher mCherry density than did LAP1, LAP1_2, and EF1α (Figure 2O). Furthermore, in striatum (Figure 2H), thalamus (Figure 2J), midbrain, motor, and sensory areas (Figures 2L and 2M), and hindbrain (Figure 2N), LAP2 and LAP1_2 showed significantly higher density than that of EF1α ($p < 0.05$). Note that the LAP2 nucleotide sequence is 68% shorter than that of EF1α, yet it outperforms EF1α density in several brain areas. To further validate LAP transgene expression in the CNS, we assessed mCherry protein expression by immunohistochemistry (IHC) in brain sagittal sections at 30 and 190 dpi (Figures 3A–3D). Analysis by confocal microscopy showed abundant mCherry staining throughout the cortical somatosensory area (Figures 3E1–3E4), dentate gyrus in the hippocampal formation (Figures 3F1–3F4), caudoputamen in the striatum (Figures 3G1–3G41), and cerebellar cortex (Figures 3H1–3H4) at 30 dpi. Importantly, mCherry expression was stable for all three LAP variants at 190 dpi and similar to that of the large promoter EF1α (Figures 3E5–3E8, 3F5–3F8, 3G5–3G8, and 3H5–3H8). Next, we quantified mCherry expression at 30 and 190 dpi. The mCherry RFI was similar for all AAV promoters with no

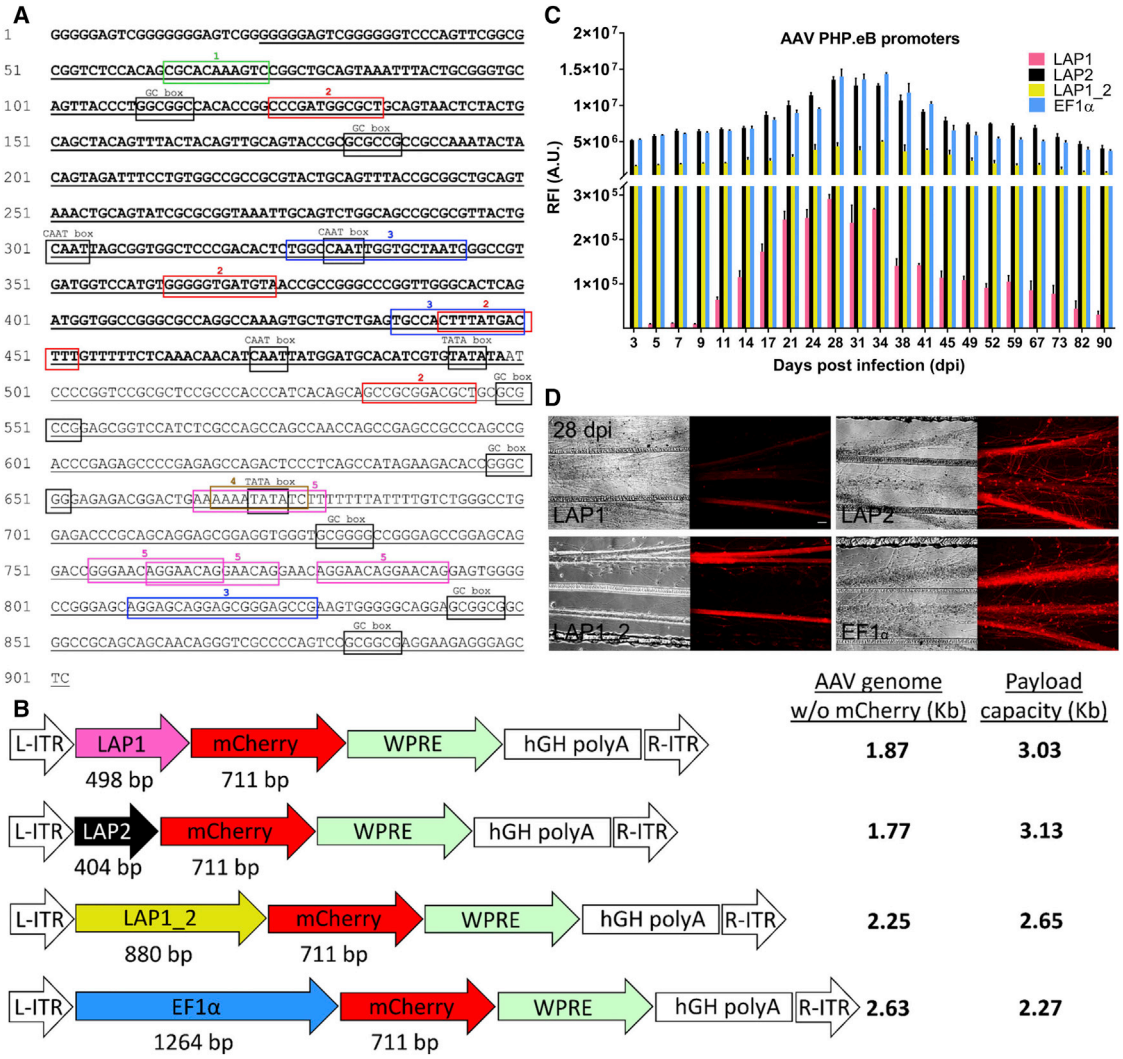

Figure 1. Characterization of PRV Latency-Associated Transcript Promoter (LAP)

(A) The complete nucleotide sequence of PRV LAP of 902 bp and the sub-regions LAP1 (bold and underlined) of 498 bp, LAP2 (underlined) of 404 bp, and LAP1_2 of 880 bp are depicted. LAP1_2 includes most of the LAP sequence, except for the first 22 nt of LAP1. Black boxes depict consensus sequences for TFs, including the GC box, specificity proteins 1 and 3 (Sp1 and Sp3); CAAT box, nuclear factor Y (NF-Y), and TATA box, TATA-binding protein (TBP). Colored boxes indicate the coordinates for TF binding motif sites as follows: 1, green, SRY-box 10 (SOX10); 2, red, cAMP response element-binding protein (CREB); 3, blue, CCCTC-binding factor (CTCF); 4, brown, oligodendrocyte transcription factor 2 (Olig2); 5, pink, signal transducer and activator of transcription (STAT1). (B) Plasmid maps of four AAVs designed to transcribe mCherry fluorescent reporter from promoters LAP1, LAP2, LAP1_2, and EF1α. WPRE of 609 bp is a woodchuck hepatitis virus posttranscriptional enhancer element. All AAVs contain a 479-bp human growth hormone (hGH poly(A)) polyadenylation sequence, as well as flanking AAV2 inverted terminal repeats (ITRs) of 141 bp each. Vectors were packaged into the AAV-PHP.eB serotype capsid. The total sizes of the enhancer-promoter elements and the promoter sequence are AAV-LAP1 (1.87 kb), AAV-LAP2 (1.77 kb), AAV-LAP1_2 (2.25 kb) and AAV-EF1α (2.63 kb), respectively. (C) All four AAVs were used to transduce primary cultures of rat SCG neurons to quantify mCherry expression during a 90-day time lapse. The relative fluorescence intensity of mCherry expression was measured at 3, 5, 7, 9, 11, 14, 17, 21, 24, 28, 31, 34, 38, 41, 45, 49, 52, 59, 67, 73, 82, and 90 days post-infection (dpi) with 3×10^{11} vg. Data are represented as mean ± SEM; n = 3 SCG culture dishes per group. (D) AAV-driven mCherry expression in SCG neurons is shown at 28 dpi with LAP1-mCherry, LAP2-mCherry, LAP1_2-mCherry, and EF1α-mCherry. Scale bar, 500 μm.

significant differences ($p < 0.05$) (Figures 3I1–3I4). We subsequently quantified the number of mCherry-positive cells per pixel^2 at 190 dpi. In the cortex, the number of LAP2-mCherry expressing cells was higher than those observed for LAP1-mCherry and LAP1_2-mCherry (LAP2, 297 ± 19.82 versus LAP1, 149 ± 5.61 versus LAP1_2, 168 ± 9.22 [n = 6, $p < 0.001$]) (Figure 3J1). In dentate gyrus, striatum, and cerebellum the number of mCherry-positive cells was similar for all LAP variants and EF1α (Figures 3J2–3J4). We conclude that all AAV-LAP variants promote mCherry expression in the brain, further demonstrating that a single administration of AAV-LAP recombinants is sufficient to drive long-term, pan-neuronal transgene expression in the mouse CNS.

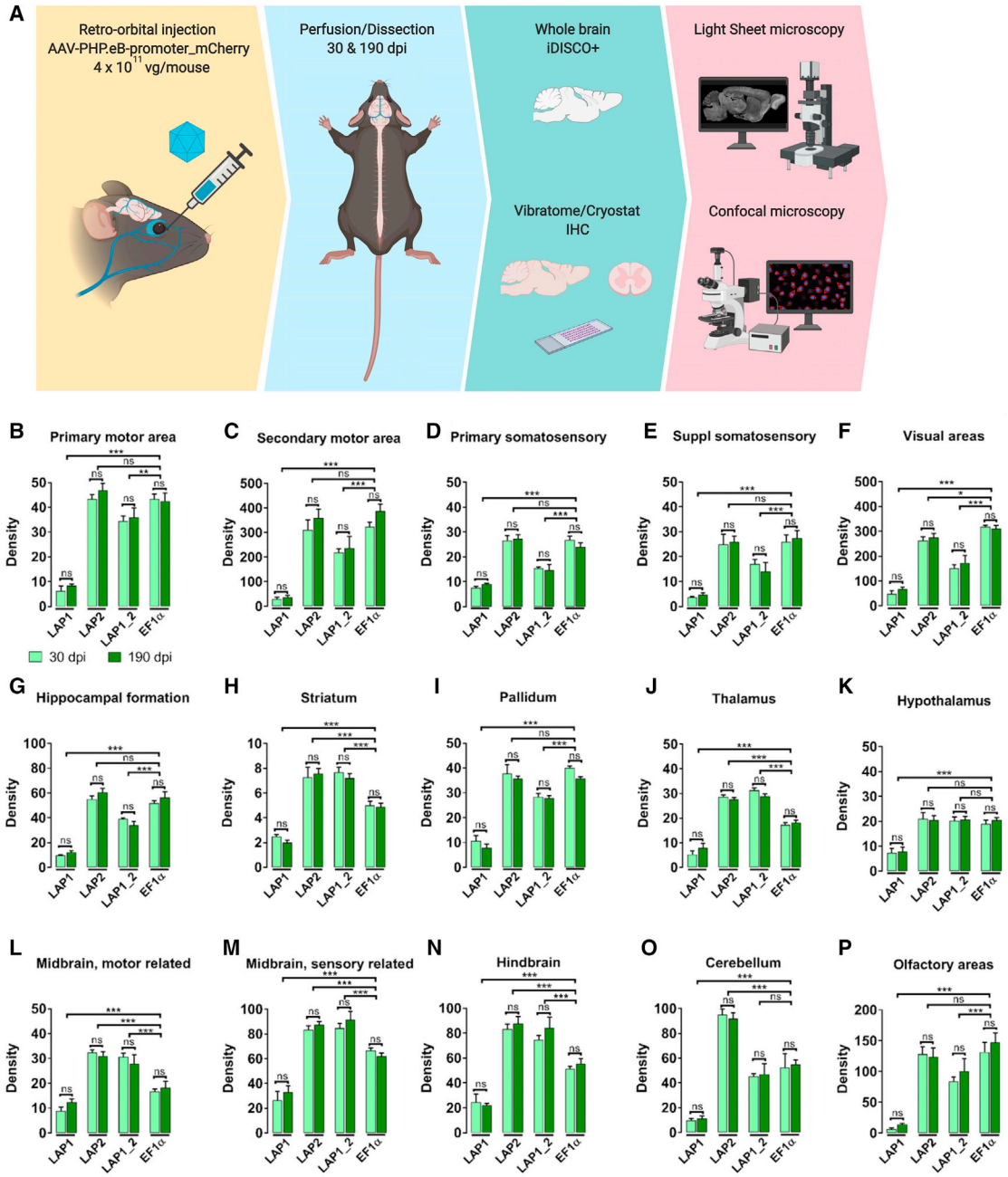

Figure 2. Whole-Brain Volumetric Registrations of AAV-Infected Animals Show Stable and Long-Term LAP-Mediated Transgene Expression

(A) Schematic of the systemic route of AAV administration and subsequent CNS tissue processing. Intravenous administration of AAV vectors was performed by unilateral injection into the mice retro-orbital sinus (4×10^{11} vg/mouse). Brain and spinal cord were collected at 30 and 190 dpi. Brain right hemispheres were processed for iDISCO+ tissue clearing and subsequent light-sheet microscopy analysis. The left hemispheres were sagittally sectioned at 50 μm for subsequent IHC and confocal microscopy analyses. Spinal cords were transversally sliced at 20 μm for subsequent confocal microscopy analyses. The image was created with biorender.com under a paid subscription. (B–P) Quantification of the density of mCherry-positive cells per mm^3 across different brain regions in iDISCO+ tissue-cleared samples at 30 and 190 dpi. Cortex area: (B) primary motor area, (C) secondary motor area, (D) primary somatosensory area, (E) supplemental somatosensory area, (F) visual areas; (G) hippocampal formation; (H) striatum; (I) pallidum; (J) thalamus; (K) hypothalamus; midbrain area: (L) motor related, (M) sensory related; (N) hindbrain; (O) cerebellum; (P) olfactory areas. Data were normalized to a vehicle-injected control animal. Data are represented as mean ± SEM; n = 2 animals per group. Between five and ten 500-μm vol per region were analyzed for each animal. Data were normalized to a vehicle-injected control animal. Significance was determined with Student's t test (when only two groups were compared) or one-way analysis of variance (ANOVA) followed by a Bonferroni *post hoc* test (when more than two groups were compared). A p value <0.05 was considered to be statistically significant (*$p < 0.033$, **$p < 0.002$, ***$p < 0.001$).

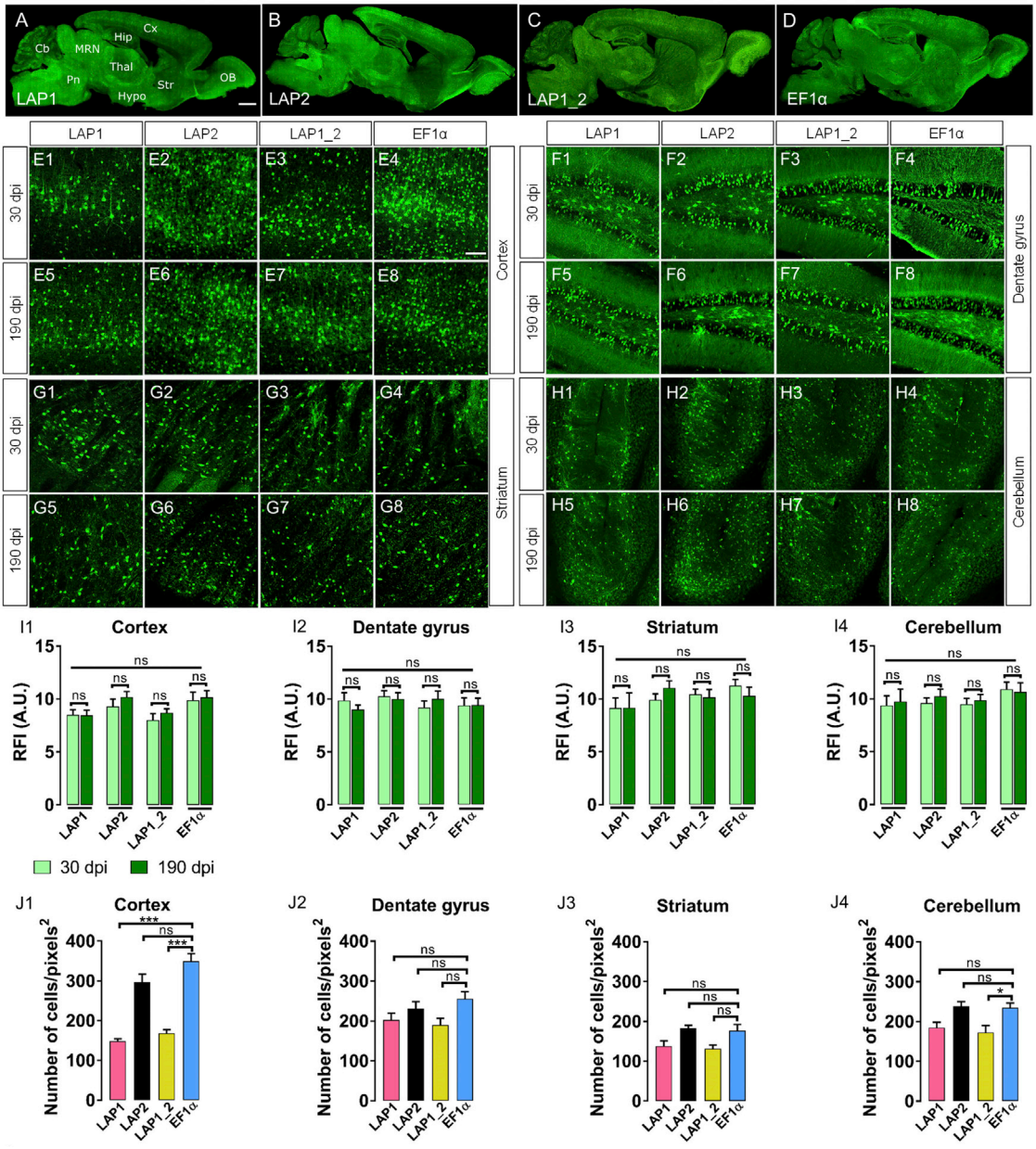

Figure 3. All Three AAV-LAP-mCherry Variants Exhibit Widespread and Long-Term Transgene Expression Throughput the Brain after Retro-Orbital Injection

(A–D) Representative immunofluorescence images of sagittal sections showing whole-brain distribution of anti-mCherry staining are shown in green for (A) AAV-LAP1, (B) AAV-LAP2, (C) AAV-LAP1_2, and (D) AAV-EF1α at 190 dpi. Cx, cortex; Hip, hippocampus; MRN, midbrain reticular nucleus; Cb, cerebellum; Thal, thalamus; Pn, pons; Hypo, hypothalamus; Str, striatum; OB, olfactory bulb. Scale bar, 1 mm. (E–H) Representative confocal images show anti-mCherry signal (green) for AAV-LAP1 (E1 and E5) in cortex, (F1 and F5) dentate gyrus, (G1 and G5) striatum and (H1 and H5) cerebellum at 30 and 190 dpi, respectively. AAV-LAP2 (E2 and E6) in cortex, (F2 and F6) in the dentate gyrus, (G2 and G6) in the striatum, and (H2 and H6) in cerebellum at 30 and 190 dpi, respectively. AAV-LAP1_2 (E3 and E7) in cortex, (F3 and F7) in the dentate gyrus, (G3 and G7) in the striatum, and (H3 and H7) in cerebellum at 30 and 190 dpi, respectively. AAV-EF1α (E4 and E8) in cortex, (F4 and F8) in the dentate gyrus, (G4 and G8) in the striatum, and (H4 and H8) in cerebellum at 30 and 190 dpi, respectively. All images are stacked confocal sections. Scale bar, 100 μm. (I and J) Quantification of the indirect fluorescence intensity of anti-mCherry signal driven by AAV-LAP variants and AAV-EF1α at 30 and 190 dpi is shown in (I1) cortex, (I2) dentate gyrus, (I3) striatum, and (I4) cerebellum. Quantification of the number of cells expressing mCherry signal per pixel^2 by IHC at 190 dpi is shown in (J1) cortex, (J2) dentate gyrus, (J3) striatum, and (J4) cerebellum. Data are represented as mean ± SEM; n = 2 (six tissue sections were analyzed for each animal). For (A), data were normalized to a vehicle-injected control animal. Significance was determined with Student's t test (when only two groups were compared) or one-way analysis of variance (ANOVA) followed by a Bonferroni *post hoc* test (when more than two groups were compared). A p value <0.05 was considered to be statistically significant (*p < 0.033, **p < 0.002, ***p < 0.001).

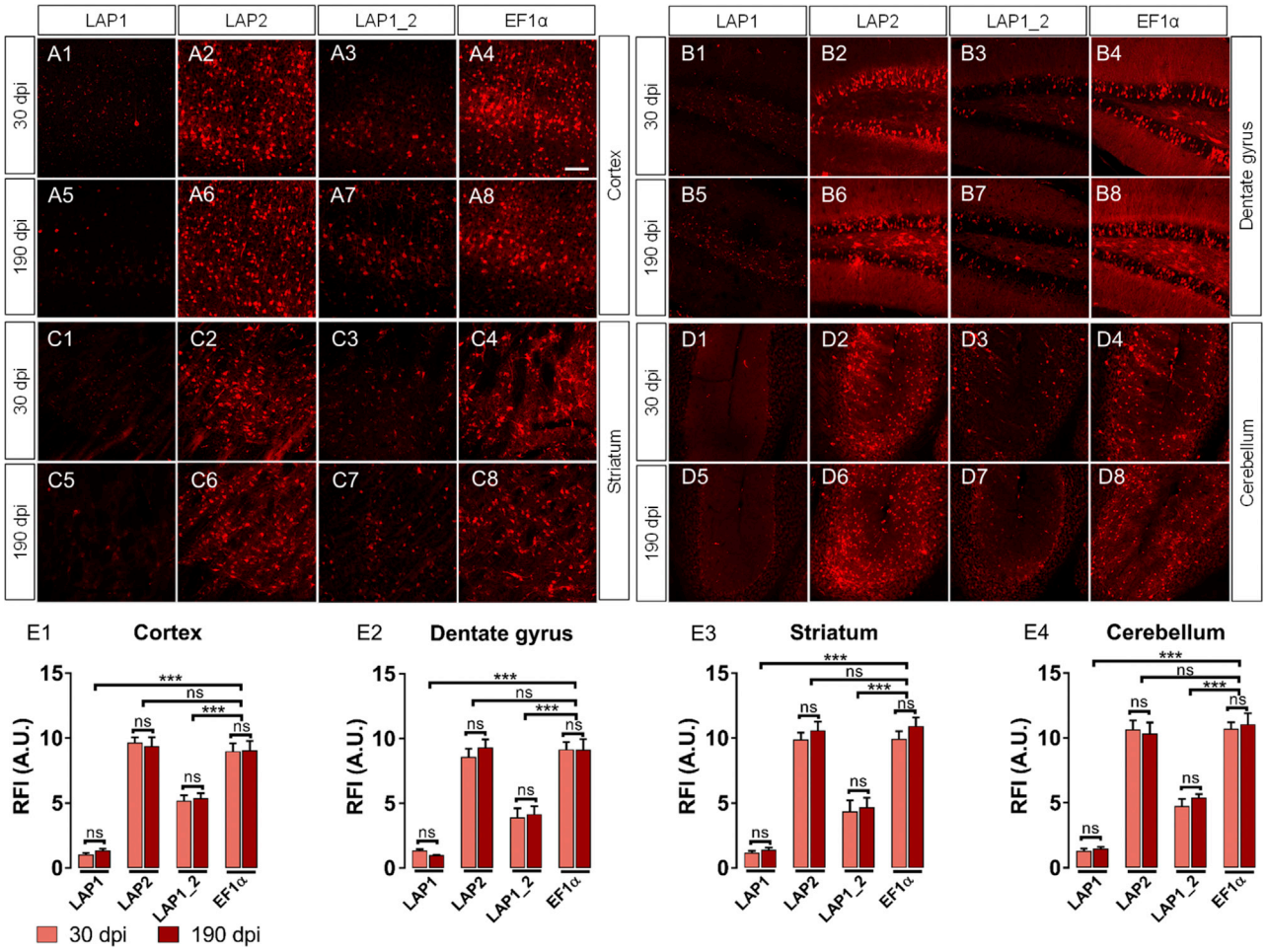

Figure 4. LAP2 Drives Stable and Long-Term Transgene Expression in the Brain

(A–D) Representative confocal images show native mCherry fluorescence (red) for AAV-LAP1 (A1 and A5) in cortex, (B1 and B5) dentate gyrus, (C1 and C5) striatum, and (D1 and D5) cerebellum at 30 and 190 dpi, respectively; AAV-LAP2 (A2 and A6) in cortex, (B2 and B6) in the dentate gyrus, (C2 and C6) in the striatum, and (D2 and D6) in cerebellum at 30 and 190 dpi, respectively; AAV-LAP1_2 (A3 and A7) in cortex, (B3 and B7) in the dentate gyrus, (C3 and C7) in the striatum, and (D3 and D7) in cerebellum at 30 and 190 dpi, respectively; and AAV-EF1α (A4 and A8) in cortex, (B4 and B8) in the dentate gyrus, (C4 and C8) in the striatum, and (D4 and D8) in cerebellum at 30 and 190 dpi, respectively. All images are stacked confocal sections. Scale bar, 100 μm. (E) Quantification of the direct fluorescence intensity (RFI) of native mCherry signal driven by AAV-LAP variants and AAV-EF1α at 30 and 190 dpi is shown in (E1) cortex, (E2) dentate gyrus, (E3) striatum, and (E4) cerebellum. Data are represented as mean ± SEM; n = 2 (six tissue sections were analyzed for each animal) and was normalized to a vehicle-injected control animal. Significance was determined with Student's t test (when only two groups were compared) or one-way analysis of variance (ANOVA) followed by a Bonferroni *post hoc* test (when more than two groups were compared). A p value <0.05 was considered to be statistically significant (*$p < 0.033$, **$p < 0.002$, ***$p < 0.001$).

The Small LAP2 Promoter Variant Drives Strong and Stable Pan-Neuronal Transgene Transcription and Translation after Systemic AAV Administration

We compared the efficacy of mCherry expression under the control of different PRV LAP variants and observed abundant signal in the cortex (Figures 4A1–4A8 and 4E1), dentate gyrus (Figures 4B1–4B8 and 4E2), striatum (Figures 4C1–4C8 and 4E3), and cerebellum (Figures 4D1–4D8 and 4E4) at 30 and 190 dpi. Moreover, the AAV-LAP2 RFI was stable and similar to that of AAV-EF1α both at 30 and 190 dpi ($p < 0.05$) (Figures 4E1–4E4; Table 1). Although AAV-LAP1 and AAV-LAP1_2 mCherry RFI levels were stable and not significantly different at 30 and 190 days in cortex, dentate gyrus, striatum, and cerebellum (Figures 4E1–4E4; Table 1), both promoters showed significantly less transgene expression (RFI) compared to LAP2 and EF1α.

Since mRNA half-life is typically shorter than that of the translated protein,[39] we measured mCherry transcripts in AAV-LAP2- and AAV-EF1α-transduced brains at 190 dpi with an mCherry-specific Riboprobe. Fluorescence *in situ* hybridization (FISH) showed abundant AAV-LAP2 mCherry RNA in cortex, dentate gyrus, striatum, cerebellum, and olfactory bulb (Figure 5), further confirming that PRV LAP2 can drive chronic and robust transgene transcription in the CNS.

Table 1. mCherry Expression in the Mouse Brain with Different AAV-PHP.eB Promoters

		Direct mCherry Expression		Indirect IHC mCherry expression	
		30 dpi	190 dpi	30 dpi	190 dpi
Promoter	Brain Region	Mean (RFI) ± SEM	Mean (RFI) ± SEM	Mean (RFI) ± SEM	Mean (RFI) ± SEM
LAP1	cortex	1.05 ± 0.12	1.35 ± 0.14	8.51 ± 0.47	8.46 ± 0.49
	dentate gyrus	1.36 ± 0.11	0.99 ± 0.04	9.87 ± 0.72	9.00 ± 0.44
	striatum	1.18 ± 0.13	1.41 ± 0.18	9.14 ± 0.97	9.17 ± 1.41
	cerebellum	1.31 ± 0.17	1.48 ± 0.15	9.38 ± 0.92	9.75 ± 1.16
LAP2	cortex	9.66 ± 0.41	9.39 ± 0.69	9.30 ± 0.70	10.18 ± 0.51
	dentate gyrus	8.61 ± 0.63	9.32 ± 0.63	10.26 ± 0.52	10.01 ± 0.59
	striatum	9.91 ± 0.51	10.61 ± 0.65	9.92 ± 0.57	11.06 ± 0.66
	cerebellum	10.66 ± 0.67	10.34 ± 0.84	9.59 ± 0.50	10.26 ± 0.65
LAP1_2	cortex	5.18 ± 0.43	5.36 ± 0.39	8.01 ± 0.61	8.70 ± 0.36
	dentate gyrus	3.92 ± 0.70	4.17 ± 0.62	9.20 ± 0.64	10.02 ± 0.72
	striatum	4.36 ± 0.84	4.67 ± 0.75	10.45 ± 0.48	10.17 ± 0.75
	cerebellum	4.76 ± 0.54	5.42 ± 0.27	9.48 ± 0.56	9.86 ± 0.54
EF1α	cortex	8.99 ± 0.62	9.05 ± 0.73	9.87 ± 0.77	10.16 ± 0.62
	dentate gyrus	9.16 ± 0.57	9.16 ± 0.81	9.40 ± 0.72	9.45 ± 0.64
	striatum	9.96 ± 0.59	10.93 ± 0.67	11.26 ± 0.61	10.29 ± 0.85
	cerebellum	10.72 ± 0.49	11.06 ± 0.84	10.92 ± 0.66	10.65 ± 0.89

IHC, immunohistochemistry; dpi, days post-injection (with AAV); RFI, relative fluorescence intensity.

AAV-LAP Transgene Expression in the Brain Is Predominant in Neurons but Not in Glial Cells

The tropism and specificity of AAV transduction and subsequent transgene expression depends on the AAV serotype 3, serotype 4, and the gene promoter 6. To characterize which cell types showed AAV-LAP-mCherry expression after systemic AAV-PHP.eB delivery, we performed co-immunostaining of mCherry protein with markers for neurons (NeuNs), oligodendrocytes (Olig2), microglia (Iba1), and astrocytes (S100) in cortex and dentate gyrus. Co-staining with NeuN and mCherry revealed that more than 88% of the neurons imaged expressed mCherry driven by the different AAV-LAP variants in both cortex and dentate gyrus (Figures 6A1–6A4, 6B1–6B4, and 6E). Conversely, less than 4% of mCherry-positive oligodendrocytes were detected for all LAP variants (Figures 6C1–6C4, 6D1–6D4, and 6F). Moreover, we observed no co-labeling of mCherry with microglia (Iba1) and astrocyte (S100) markers for any of the AAV-LAP recombinants (Figure S1). Overall, these results demonstrate that at least in the context of systemic brain transduction with AAV-PHP.eB, LAP-mCherry expression is abundant in neurons but not in glial cells.

AV-LAP Constructs Exhibit Broad, Stable, and Long-Term Transgene Expression throughout the Spinal Cord

In addition to the brain, we evaluated AAV-LAP performance in the spinal cord, where the serotype PHP.eB has shown widespread transduction of gray matter.[5,6] We observed abundant native mCherry expression in both dorsal and ventral horns of the spinal cord at the cervical, thoracic, and lumbar levels at 190 dpi (Figures 7A–7D). Native mCherry RFI was similar for all promoters with no statistically significant differences ($p < 0.05$) (Figure 7E). However, LAP2 and LAP1_2 recombinants showed the highest density of mCherry-positive cells per pixel^2, followed by EF1α and LAP1, respectively; that is, LAP2 = LAP1_2 > EF1α > LAP1 (Figure 7F). Therefore, all three PRV LAP variants effectively mediate pan-neuronal, long-term transgene expression in the spinal cord.

DISCUSSION

Gene therapy has been used to restore gene function in specific target cells in neurological disorders.[40] Gene transfer by systemic vector delivery via peripheral vascular transduction can be difficult for efficient expression in a neuron-specific or pan-neuronal fashion in the CNS.[41] Recombinant AAV vectors are among the most efficient vehicles to achieve gene expression in the CNS.[1,42] Moreover, engineered AAV capsids have shown improved CNS transduction and enhanced capacity to cross the BBB with higher efficiency than naturally occurring serotypes.[4,5] Despite these advances, AAV gene therapy is hindered by the small payload size limit of only 4.9 kb.[43] For example, CNS therapies for Pompe disease[44] and Parkinson's disease[45] are based on delivery of relatively large genes such as GAA (2.9 kb) and GDNF (2.5 kb). For these and other similar cases, small, non-repressible promoters are ideal replacements for larger promoters or even smaller CMV and hSyn promoters shown to be quickly repressed after delivery.[12,13]

We identified three small pan-neuronal promoters isolated from the genome of the alphaherpesvirus PRV, showing efficient and long-term transgene expression in the mouse CNS after systemic AAV

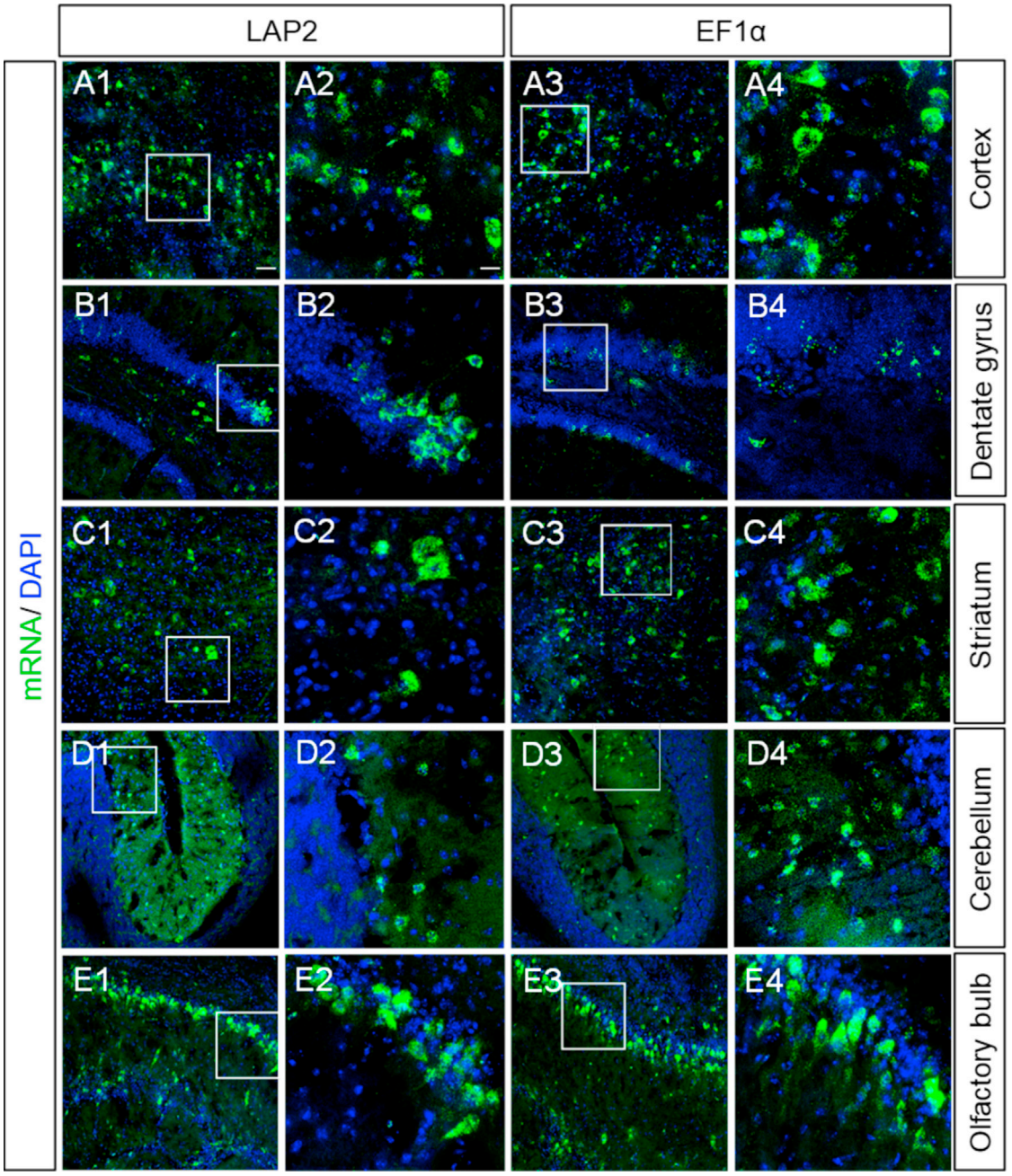

Figure 5. AAV-LAP2 Drives Long-Term Transgene Transcription in the CNS

The presence of mCherry mRNA was verified by FISH in brain tissue at 190 dpi using a riboprobe specific to mCherry (green). Nuclei were counterstained with DAPI (blue). (A–E) Brain sagittal 20-μm slices are shown for AAV-LAP2 and AAV-EF1α (A) in cortex, (B) dentate gyrus, (C) striatum, (D) cerebellum, and (E) olfactory bulb, respectively. A2, A4, B2, B4, C2, C4, D2, D4, E2, and E4 are higher magnification images (white square) of each region from A1, A3, B1, B3, C1, C3, D1, D3, E1, and E3, respectively. Images are stacked confocal sections: Scale bars, 50 and 100 μm.

PHP.eB delivery. Our results demonstrate that these small PRV LAP variants can drive long-term expression of a reporter transgene (>6 months) in brain and spinal cord. PRV LAPs uniformly transduced neurons in the cortex, striatum, dentate gyrus, and cerebellum. The distribution of mCherry-positive cells was not significantly different between LAP variants in the dentate gyrus, striatum, and cerebellum. However, LAP2 transgene expression was significantly higher in cortex compared to that of LAP1 and LAP1_2, respectively. Our whole-brain screening assay demonstrated that the LAP2 variant of only 402 bp can drive stronger mCherry expression than larger

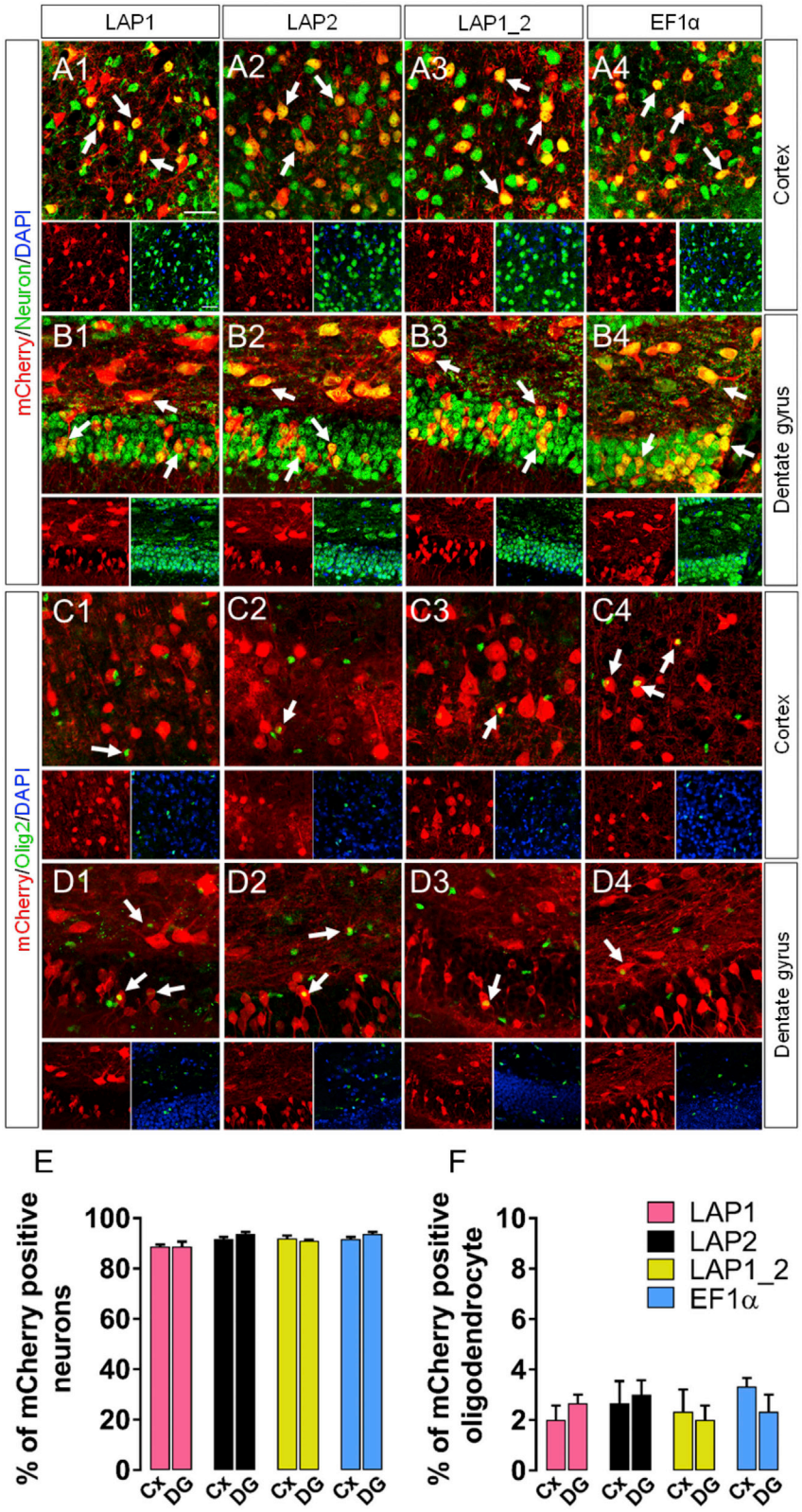

Figure 6. AAV-LAP Transgene Expression is Predominantly Expressed in Neurons and Not in Oligodendrocytes

(A–D) Representative confocal images of (A and B) AAV-mediated mCherry expression (red) in neurons (green label for the pan-neuronal marker NeuN) and (C and D) oligodendrocytes (green label for the oligodendrocyte marker Olig2), in both cortex and dentate gyrus, at 30 dpi. Cells were counterstained with DAPI (blue). The NeuN signal can localize with the neuronal cell nucleus as well as the cytoplasm, while the staining for the Olig2 signal is mostly nuclear. Arrows depict co-labeling between the cell marker and mCherry. (A1 and C1) AAV-LAP1 in cortex, (B1 and D1) AAV-LAP1 in dentate gyrus; (A2 and C2) AAV-LAP2 in cortex, (B2 and D2) AAV-LAP2 in dentate gyrus; (A3 and C3) AAV-LAP1_2 in cortex, (B3 and D3) AAV-LAP1_2 in dentate gyrus; (A4 and C4) AAV-EF1α in cortex, (B4 and D4) AAV-EF1α in dentate gyrus. Scale bar, 100 μm. (E and F) Quantification of the percentage of (E) AAV-mCherry labeled cells corresponding to neurons (NeuN-positive) or (F) oligodendrocytes (Olig2-positive) in cortex (Cx) or dentate gyrus (DG) for each promoter, respectively. Images are stacked confocal sections. Data are represented as mean ± SEM; n = 2 (six tissue sections were analyzed per animal).

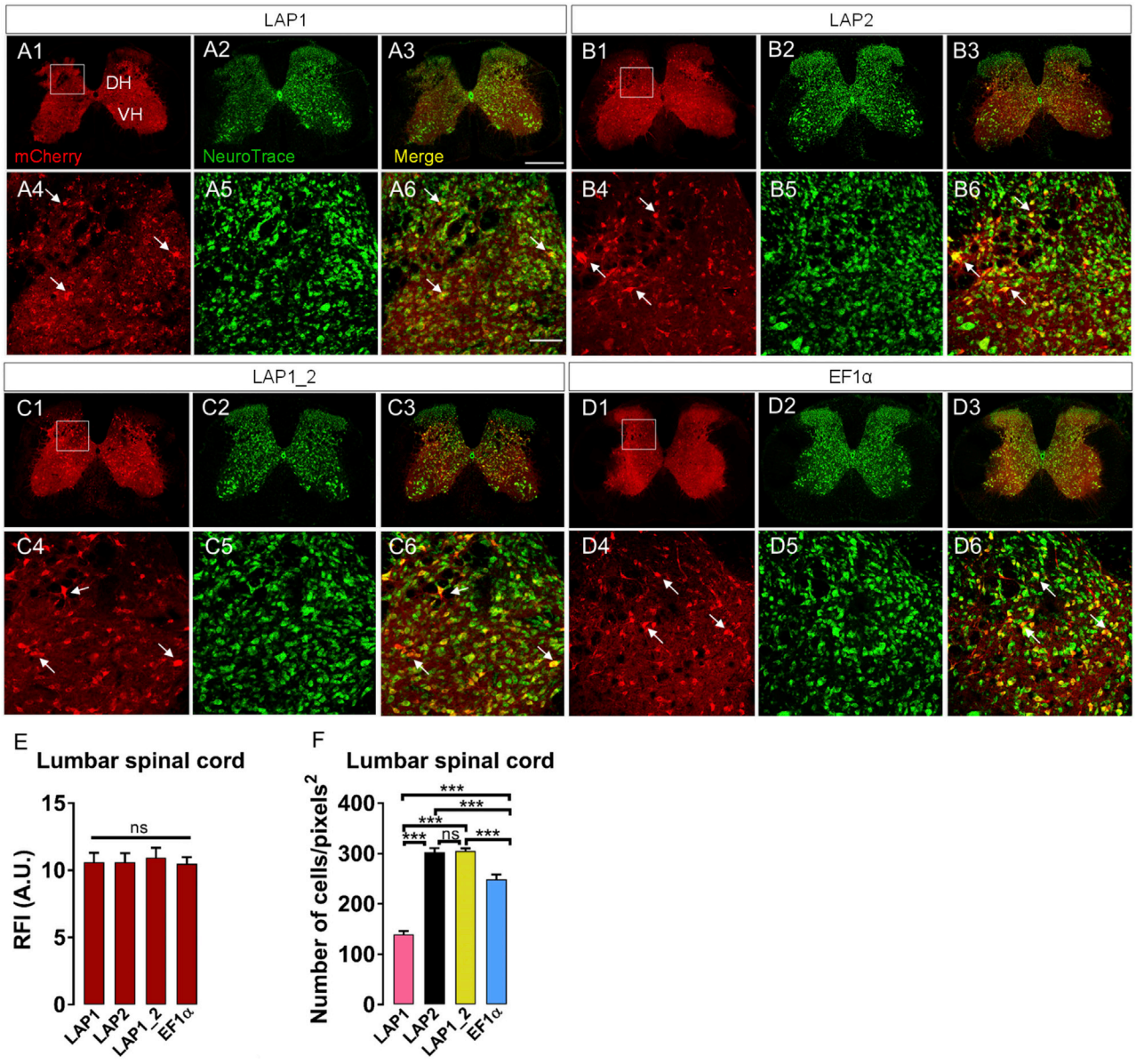

Figure 7. LAP Drives Widespread and Long-Term Transgene Expression in the Spinal Cord

Spinal cords (lumbar region) were sectioned in a transversal fashion at 20 μm. Representative 190 dpi confocal images from native AAV-mediated mCherry expression (red), pan-neuronal marker NeuroTrace (green), and merge signal (yellow) are shown for (A1–A3) AAV-LAP1, (B1–B3) AAV-LAP2, (C1–C3) AAV-LAP1_2, and (D1–D3) AAV-EF1α. DH, dorsal horn; VH, ventral horn. Higher magnification images of the DH are shown for (A4–A6) AAV-LAP1, (B4–B6) AAV-LAP2, (C4–C6) AAV-LAP1_2, and (D4–D6) AAV-EF1α, respectively. Images are stacked confocal sections. Scale bars, 1 mm and 100 μm. (E) Quantification of the direct fluorescence intensity (RFI) of native mCherry signal driven by AAV-LAP variants and AAV-EF1α at 190 dpi. (F) Quantification of the number of cells expressing mCherry signal per pixel^2 at 190 dpi is shown for AAV-LAP variants and AAV-EF1α. Significance was determined with analysis of variance one-way (ANOVA) followed by Bonferroni post hoc test. A p value < 0.05 was considered to be statically significant (*p < 0.033; **p < 0.002; ***p < 0.001).

LAP1 and LAP1_2 sequences. Moreover, we detected abundant mCherry mRNA transcribed from LAP2 in every screened brain region at 190 dpi. These results demonstrate both efficient transcription and translation driven from the small PRV LAP2 in the CNS after systemic AAV-LAP2 delivery in the absence of PRV infection. Although LAP1-mCherry cell density was significantly lower than that of LAP2, mCherry expression remained stable and long-lasting. Therefore, LAP1 might be useful in cases where low amounts of the therapeutic protein are needed (e.g., enzyme deficiencies), or cross-correction to non-transduced cells, relevant in lysosomal enzyme deficiencies[17] and

mucopolysaccharidosis VII diseases,[46] where the enzyme restored by AAV therapy can be secreted from the transduced cell to cure neighboring diseased cells.

Efficient transgene expression either in a broad or cell type-specific fashion requires binding and action of cell-derived TFs to the promoter region.[6,47] Changes in the neuronal environment such as aging or differentiation can also alter the recruitment of cell-specific regulatory proteins and therefore gene expression in the CNS.[48] Our analysis of the PRV LAP sequence identified DPEs in LAP2, which could control transgene expression onset, duration, and cell-type specificity. Additionally, we identified four STAT1 motifs that in HSV-1 LAPs seem to regulate viral reactivation from latency.[49] Strikingly, we identified one of these STAT1 motifs in the PRV LAP2 sequence, co-localizing with the TATA box and an Olig2 motif.[50] The proximity effects associated with these motifs and the transcriptional start site could explain the different levels of CNS transgene expression between LAP2, LAP1, and LAP1_2. However, further investigation of these regulatory elements is required to understand the fine-tuning of PRV LAP2 transcriptional activity. Additionally, we found one CTCF motif downstream of the LAP2 TATA box, which could have a role in the resistance to epigenetic silencing during latency, as shown for HSV-1.[51,52] Indeed, Zimmerman et al.[53] found that insertion of a CTCF motif downstream of the EF1α promoter sequence increased transgene expression significantly compared to native EF1α and CMV promoters. Interestingly, the insertion of a secondary CTCF motif downstream of the CMV TATA box had no effect on luciferase reporter expression, presumably due to the redundant presence of a native CTCF motif.[53] Accordingly, gene expression is susceptible to changes depending on the genetic context and sequence-specific DNA binding proteins. The recruitment of specific TFs from different host cells can modulate transgene transcription by the same mechanisms regulating resistance to inactivation during latency. Insulator elements such as the CTCF-binding factor are independently regulated[54] and can protect promoter regions from repression by heterochromatin, maintaining long-lasting transcription.[51]

AAV tropism is determined primarily by interactions between the capsid and specific receptors in susceptible and permissive cells.[3,4] However, the promoter sequence and other sequences included in the vector such as the inverted terminal repeat (ITR) sequence can have a substantial impact on tropism.[55] Histological assessment of cell-specific transduction by colocalization of LAP-mCherry, glial and neuronal markers, revealed that LAP variants express more efficiently in neurons than glia both in cortex and dentate gyrus. LAP-mCherry-positive cells colocalized predominantly with neuron-specific markers, and to a lesser extent with oligodendrocytes but not microglia or astrocytes. Based on these findings, we conclude that PRV LAP sequences have a pan-neuronal promoter profile in the CNS after PHP.eB systemic delivery. The same profile has been reported for HSV LAPs due to the presence of a CRE motif upstream of the TATA box.[56,57] Transgenic mouse lines containing PRV LAP1 and LAP2 sequences demonstrated that LAPs are neuron-specific promoters in the absence of other viral proteins and that neuronal TFs are sufficient to activate LAPs *in vivo*.[32] Importantly, AAV-PHP.eB transduces neurons predominantly,[5] and the combination of this capsid variant with PRV LAP sequences exhibits a strong, long-lasting, pan-neuronal expression profile in the CNS. Future research should asses the transgene expression profile of PRV LAPs with additional AAV serotypes in tissues/organs other than the CNS and in animal models other than rodents. We predict that PRV LAPs can be used not only in the context of recombinant viral vectors (AAV, adenovirus, lentivirus, herpesvirus), but also with non-viral gene delivery platforms. The natural host of PRV is the adult swine, but the virus has an extremely broad tropism and can infect some birds, fish, and many types of mammals, including some primates.[58] Moreover, human cells in culture are susceptible to PRV infection, and there are reports of zoonotic infections.[59] Therefore, the PRV LAP sequence could be naturally optimized for gene therapy applications requiring efficient and long-term transgene expression in several different mammals, including humans.

Given that the LAP2-mCherry AAV plasmid is ~2,500 bp, it is possible that packaged AAV capsids correspond to a heterogeneous population of both single-stranded (ssAAV) and self-complementary (scAAV) genomes. This could have led to potential overestimation of LAP2-mCherry expression when compared to the larger EF1a-mCherry AAV plasmid, which is less prone to dimerizing into scAAV. We expect to address this possibility in future experiments. However, we consider the smaller size of LAP2 as an advantage for future therapeutic applications where faster onset of transgene expression could be achieved with scAAV vectors that do not require the rate-limiting second strand synthesis step of ssAAV.[12,60,61] Although scAAVs are further restricted in their payload capacity, they could potentially boost transgene expression while lowering the viral dose required for efficient transduction.[61] The use of enhancer elements is another option to increase expression and decrease viral dose and viral-dependent toxicity. The woodchuck hepatitis virus posttranscriptional regulatory element (WPRE) of 609 bp is a dispensable enhancer element commonly used in AAV vectors studying the nervous system and other organs.[18,62] We are aware that WPRE is not typically used in the context of human AAV gene therapy given the payload constrains. Moreover, the enhancing effect of the WPRE does not seem to be consistent for all promoters.[63,64] Nevertheless, it has been shown that WPRE can prevent transgene repression of CAG and CMV promoters, respectively.[65,66] Given the aforementioned payload constrains, a smaller WPRE variant of only 247 bp[67] would be worth testing in future experiments. In summary, we have demonstrated that PRV LAP activity is independent of PRV infection and found that small AAV-PHP.eB-LAP variants express transgenes in a stable and pan-neuronal fashion in brain and spinal cord. Long-term transgene transcription and translation are paramount for effective and long-lasting single-dose gene therapy applications, especially when AAV treatments are provided to newborns, and it is expected to last 80 or more years. Thus, PRV LAPs may be useful for the treatment of genetic CNS diseases after one-time viral-vector administration.

MATERIALS AND METHODS

Construction of PRV LAPs

The PRV LAP was PCR amplified from coordinates 95106–96007 of PRV Becker strain genome (GenBank: JF797219.1). The LAP1 region (498 bp) was amplified using primer pairs LAP1 forward (5′-GCA CGC GTA TCT CCG GAA AGA GGA AAT TGA-3′) and LAP1 reverse (5′-GCG GAT CCT ATA TAC ACG ATG TGC ATC CAT AAT-3′). The LAP2 region (404 bp) was amplified using primer pairs LAP2 forward (5′-GCA CGC GTA TCC CCG GTC CGC GCT CCG CCC ACC CA-3′) and LAP2 reverse (5′-GCG GAT CCG AGC TCC CTC TTC CTC GCC GCG GAC TGG-3′). LAP1_2 (902 bp) spanning the entire LAP region was amplified using LAP1 forward and LAP2 reverse.[26] The 5′ and 3′ regions of these PCR sequences contained the MluI and BamHI restriction sites, respectively, used for directional cloning into vector pAAV-EF1α-mCherry. The three AAV-LAP plasmids were constructed by double digestion of vector pAAV-EF1α-mCherry with MluI and BamHI followed by subcloning of the appropriate LAP fragment upstream of the mCherry reporter gene, flanked by AAV2 ITRs and terminated with the SV40 poly(A) signal. pAAV-EF1α-mCherry was a gift from Karl Deisseroth (Addgene plasmid #114470).

Construction of AAV Vectors

All expression cassettes were packaged into AAV-PHP.eB capsids (gift from Daniela Gradinaru, Addgene plasmid #103005) at the Princeton Neuroscience Institute Viral Core Facility and purified by iodixanol step gradient and column ultrafiltration as previously described.[5,68] Capsid-protected viral genomes were measured by TaqMan qPCR and reported as genome copies (GC)/mL.

Animals

Animal studies were performed following guidelines and protocols approved by the Institutional Animal Care and Use Committee of Princeton University (protocols 1943-16 and 1047). Timed-pregnant Sprague-Dawley rats were obtained from Hilltop Labs (Scottdale, PA, USA). Adult (4- to 6-week-old) wild-type C57BL/6J male mice were obtained from The Jackson Laboratory (Bar Harbor, ME, USA). Mice had at least 48 h of acclimation to the holding facility in the Princeton Neuroscience Institute vivarium before experimental procedures were performed.

Primary Superior Cervical Ganglia Cell Culture

SCG neurons from rat embryos (embryonic day 17 [E17]) were cultured in trichambers as previously described.[69] Briefly, SCGs were dissociated with trypsin (2.5 mg/mL, Sigma-Aldrich, The Woodlands, TX, USA) and plated on poly-*O*-ornithine and laminin-coated dishes with media containing neurobasal media supplemented with 2% B-27, 100 ng/mL nerve growth factor (NGF), and 1% penicillin-streptomycin-glutamine (Thermo Fisher Scientific, Rockford, IL, USA). Approximately two-thirds of a single ganglion was placed for the S (soma) compartment of the trichamber. Three days after seeding, culture medium was treated with 0.1 mM cytosine-D-arabinofuranoside (Ara C) (Sigma-Aldrich, The Woodlands, TX, USA) for at least 2 days to eliminate dividing, nonneuronal cells. Culture media were replaced every 5 days, and neurons were incubated at 37°C with 5% CO_2.

Retro-Orbital Sinus Injection

Intravenous administration of AAV vectors was performed in mice by unilateral injection into the retro-orbital venous sinus.[70] Animals were anesthetized using a ketamine (80 mg/kg)/xylazine (10 mg/kg) cocktail prior to the procedure. Once unresponsive, animals were placed in lateral recumbence for injection into the medial canthus. Injection volume was 100 μL containing a total of 4×10^{11} vg administered with a 29G × 1/2-inch insulin syringe. Animals were placed on regulated heating pads and monitored until ambulant.

Tissue Processing and Histological Procedures

Mice were anesthetized with an overdose of ketamine (400 mg/kg)/xylazine (50 mg/kg) intraperitoneally (i.p.) and perfused with 4% paraformaldehyde (PFA) at 30 and 190 dpi. Brain and spinal cord were post-fixed for 2 h in 4% PFA at RT (room temperature). After rinsing with phosphate-buffered saline (PBS), brains were divided into two parts. Right hemispheres were used for the iDISCO+ tissue-clearing protocol (below). Left-brain hemispheres and spinal cords were serially incubated in 10% sucrose, 20% sucrose, and 30% sucrose overnight at 4°C. Tissue was placed in an embedding mold (Sigma-Aldrich, The Woodlands, TX, USA) with OCT (Tissue-Tek, Torrance, CA, USA), frozen in dry ice, and stored at −80°C until it was cryosectioned. Left hemispheres were sagittally sectioned at 50 μm using a Leica VT1200 vibratome for IHC and at 20 μm using a Leica CM3050 S cryostat for RNAscope. Spinal cords were transversally sliced at 20 μm using a cryostat.

Immunostaining

For immunohistochemistry, free-floating brain sections were washed with PBS and blocked for 1 h with 3% bovine serum albumin (BSA), 2% donkey serum, and 0.5% Triton X-100 (Sigma-Aldrich, St. Louis, MO, USA). Samples were incubated with primary antibodies overnight at 4°C and secondary antibodies for 1 h at RT diluted in PBS containing 1% BSA, 1% donkey serum, and 0.5% Triton X-100. Cell nuclei were counterstained with 0.5 μg/mL DAPI for 5 min (Thermo Fisher Scientific, Rockford, IL, USA). The following primary antibodies were used: rabbit anti-RFP (red fluorescent protein) (1:1,000; Rockland, Limerick, PA, USA), chicken anti-mCherry (1:500; Abcam, Cambridge, MA, USA), mouse anti-NeuN (1:500; Millipore Bioscience Research Reagents, Temecula, CA, USA), rabbit anti-Olig2 (1:500; EMD Millipore, Temecula, CA, USA), rabbit anti-Iba1 (1:1,000; Wako Pure Chemicals Industries, Richmond, VA, USA), and rabbit anti-S100 (1:5,000; Dako, Glostrup, Denmark). The following secondary antibodies were used: Alexa Fluor 488 donkey anti-rabbit immunoglobulin G (IgG), Alexa Fluor 488 donkey anti-mouse IgG, Alexa Fluor 647 donkey anti-rabbit IgG, Alexa Fluor 647 donkey anti-chicken IgG (1:1,000; Thermo Fisher Scientific, Rockford, IL, USA). Spinal cord free-floating sections were stained with a 1:300 dilution of NeuroTrace 500/525 green fluorescent Nissl stain (Molecular Probes, Eugene, OR, USA) for 1 h. The sections were permeabilized with 0.1% Triton X-100

in PBS for 10 min and washed first with PBS followed by PBS with 0.1% Triton X-100 for 10 min. Samples were incubated with 0.5 μg/mL DAPI for 5 min and then washed with PBS for 2 h at RT. Fluoromount-G mounting medium (SouthernBiotech, Birmingham, AL, USA) was applied to brain and spinal cord sections before mounting.

Microscopy

Neuronal SCG cultures were imaged with a Nikon Ti-E inverted epifluorescence microscope (Nikon Instruments, Tokyo, Japan), containing a CoolSNAP ES2 camera (Photometrics, Tucson, AZ, USA) and ×4 objective. Tiled images of the entire S compartment were assembled with the Nikon NIS-Elements software. To quantify AAV transduction efficacy in various brain regions, brain slices were imaged with a NanoZoomer S60 fluorescent microscope scanner (Hamamatsu, Hamamatsu, Japan). Brain slices were imaged with a Leica STP8000 confocal laser-scanning microscope (Leica Microsystems, Wetzlar, Germany) using ×20 and ×63 objectives, hybrid (HyD) detectors for sensitive detection, and a 1,024 × 1,024-pixel area. Stacks of consecutive images were taken with a ×20 objective, and Z projections were reconstructed with ImageJ software to calculate corrected total cell fluorescence as previously reported.[71] Cells were selected drawing a region of interest (ROI) and normalized to background intensity from non-fluorescent cells. The calculation of corrected total cell fluorescence was measured as RFI considering area integrated, density, and mean gray value of each cell.

iDISCO+ Tissue Clearing

Permeabilization

Right-brain hemispheres were used for iDISCO+ tissue clearing. Brain samples were fixed overnight in 4% PFA prior to tissue clearing as previously described.[38] Fixed samples were washed/dehydrated in 20%, 40%, 60%, 80%, and 100% methanol/water solutions for 1 h each, followed by a 5% hydrogen peroxide/methanol overnight wash (Sigma-Aldrich, St. Louis, MO, USA) and rehydration with a reverse gradient of methanol/water at 100%, 80%, 60%, 40%, and 20% for 1 h each. Finally, brains were washed with 0.2% Triton X-100/PBS, followed by 20% DMSO (Thermo Fisher Scientific, Rockford, IL, USA)/0.3 M glycine (Sigma-Aldrich, St. Louis, MO, USA)/0.2% Triton X-100/PBS at 37°C for 2 days.

Immunolabeling

Samples were incubated in a blocking solution of 10% DMSO/6% donkey serum (EMD Millipore, Temecula, CA, USA)/0.2% Triton X-100/PBS at 37°C for 2–3 days, followed by two 1-h washes in PBS/0.2% Tween-20 (Sigma-Aldrich, St. Louis, MO, USA) with 10 μg/mL heparin (solution hereinafter referred to as PTwH, Sigma-Aldrich, St. Louis, MO, USA). Brains were incubated with primary rabbit anti-RFP antibody (1:1,000; Rockland, Limerick, PA, USA) in 5% DMSO/3% donkey serum/PTwH at 37°C for 7 days. Next, brains were washed with PTwH five times (wash intervals of 10 min, 15 min, 30 min, 1 h, and 2 h) and incubated at 37°C for 7 days with secondary Alexa Fluor 647 donkey anti-rabbit IgG (1:450; Thermo Fisher Scientific, Rockford, IL, USA) in 3% donkey serum/PTwH and then washed in PTwH five times.

Tissue Clearing

Brains were sequentially dehydrated in 20%, 40%, 60%, 80%, and 100% methanol/water for 1 h each step, followed by 2:1 dichloromethane (DCM; Sigma-Aldrich, St. Louis, MO, USA)/methanol, and 100% DCM washes. Finally, samples were cleared with dibenzyl ether (DBE; Sigma-Aldrich, St. Louis, MO, USA) and stored in the dark at RT until imaged.

Light-Sheet Microscopy and Analysis of Cleared Tissue

After immunolabeling and clearing, brain volumes were acquired using a light-sheet UltraMicroscope II (LaVision BioTec, Bielefeld, Germany). Brain halves were glued in the horizontal orientation on a custom-designed 3D-printed holder[37,38] and submerged in DBE. Brains were imaged in the autofluorescence channel for registration purposes with a 488-nm laser diode excitation and a 525-nm maximum emission filter (FF01-525/39-25, Semrock, Rochester, NY, USA), and at 640-nm excitation with a 680-nm maximum emission filter (FF01-680/42-25, Semrock) for cellular imaging of AAV-infected cells (anti-RFP). Separate left- and right-sided illumination autofluorescence images were acquired every 10 μm (z-steps size) using a 0.017 excitation-sheet numerical aperture (NA) and ×1.3 magnification. Left- and right-sided images were sigmoidally blended at the midline. Autofluorescence volumes were registered to the volumetric Allen Brain Atlas (2015) using affine and B-spline transformations, as described by Renier et al.[37,38] To account for movement during acquisition and different imaging parameters between channels, cell signal volumes were registered to autofluorescence volumes with an affine transform. Brain volumes were analyzed with our modified ClearMap software ClearMapCluster (https://github.com/PrincetonUniversity/ClearMapCluster), compatible with high-performance computing clusters. Between five and ten 500-μm vol per brain region were analyzed for each animal to obtain the average local density measurements. For all analyzed samples, detected objects on brain edges and ventricles were eroded by 75 μm from the edge of the structure to minimize false positives.

RNAscope *In Situ* Hybridization

Brain cryosections were mounted on SuperFrost Plus adhesion slides (Thermo Fisher Scientific, Waltham, MA, USA) and stored at −80°C. RNA staining was performed using the RNAscope multiplex fluorescent reagent kit (Advanced Cell Diagnostics [ACD], Newark, CA, USA) following the manufacturer's protocol. The mCherry probe ACD #431201-C2 was used. Slices were pretreated with protease IV for 30 min at 40°C, followed by probe incubation for 2 h at 40°C. Then, different amplifier solutions were performed for 30, 30, and 15 min at 40°C. Signal was detected with a tyramide signal amplification (TSA) Plus fluorescein system (PerkinElmer, Waltham, MA, USA). Incubation steps were done in the ACD HybEZ hybridization system. Slides were counterstained with DAPI for 30 s at RT. Finally, slides were mounted with Vectashield mounting medium (Vector Laboratories, Burlingame, CA, USA).

Statistical Analysis

Statistical data analysis was performed using GraphPad Prism 7 software (GraphPad, La Jolla, CA, USA). A two-tailed Student's test was

used to compare between two groups, and a non-parametric one-way ANOVA test followed by a Bonferroni multiple comparison post-test was used to compare among multiple groups. A p value <0.05 was considered to be statistically significant. Data are represented as the mean with SEM.

SUPPLEMENTAL INFORMATION

Supplemental Information can be found online at https://doi.org/10.1016/j.omtm.2020.04.004.

AUTHOR CONTRIBUTIONS

C.J.M. and E.A.E. conceived the project and designed the experiments. C.J.M. performed tissue processing, histology, immunostaining, and RNA FISH experiments, as well as primary superior cervical ganglia cell culture experiments, confocal imaging, figure preparation, and statistical analysis. T.J.P. and Z.M.D. performed iDISCO+ studies. A.E. cloned LAPs into AAV plasmids. C.J.M. and J.L.V. performed the *in vivo* retro-orbital injections. C.J.M. and E.A.E. analyzed the data. C.J.M. and E.A.E. wrote the paper. All authors contributed to critical revisions of the manuscript. E.A.E. provided study oversight. L.W.E. and E.A.E. obtained funding.

CONFLICTS OF INTEREST

The authors declare no competing interests.

ACKNOWLEDGMENTS

This work was supported by a Research Innovator Award from the Princeton Neuroscience Institute to E.A.E. and L.W.E. We thank Prof. Sam Wang for kindly sharing consumables and laboratory equipment, Dr. Mahdi Kooshkbaghi for software assistance and Angela Chan for laboratory assistance. Publication expenses were supported by NIH grant P40OD010996 to E.A.E and L.W.E.

REFERENCES

1. Hudry, E., and Vandenberghe, L.H. (2019). Therapeutic AAV gene transfer to the nervous system: a clinical reality. Neuron *102*, 263.
2. Ogden, P.J., Kelsic, E.D., Sinai, S., and Church, G.M. (2019). Comprehensive AAV capsid fitness landscape reveals a viral gene and enables machine-guided design. Science *366*, 1139–1143.
3. Aschauer, D.F., Kreuz, S., and Rumpel, S. (2013). Analysis of transduction efficiency, tropism and axonal transport of AAV serotypes 1, 2, 5, 6, 8 and 9 in the mouse brain. PLoS ONE *8*, e76310.
4. Bedbrook, C.N., Deverman, B.E., and Gradinaru, V. (2018). Viral strategies for targeting the central and peripheral nervous systems. Annu. Rev. Neurosci. *41*, 323–348.
5. Chan, K.Y., Jang, M.J., Yoo, B.B., Greenbaum, A., Ravi, N., Wu, W.L., Sánchez-Guardado, L., Lois, C., Mazmanian, S.K., Deverman, B.E., and Gradinaru, V. (2017). Engineered AAVs for efficient noninvasive gene delivery to the central and peripheral nervous systems. Nat. Neurosci. *20*, 1172–1179.
6. Dayton, R.D., Grames, M.S., and Klein, R.L. (2018). More expansive gene transfer to the rat CNS: AAV PHP.EB vector dose-response and comparison to AAV PHP.B. Gene Ther. *25*, 392–400.
7. Russell, D.W., and Hirata, R.K. (1998). Human gene targeting by viral vectors. Nat. Genet. *18*, 325–330.
8. Delzor, A., Dufour, N., Petit, F., Guillermier, M., Houitte, D., Auregan, G., Brouillet, E., Hantraye, P., and Déglon, N. (2012). Restricted transgene expression in the brain with cell-type specific neuronal promoters. Hum. Gene Ther. Methods *23*, 242–254.
9. Peel, A.L., Zolotukhin, S., Schrimsher, G.W., Muzyczka, N., and Reier, P.J. (1997). Efficient transduction of green fluorescent protein in spinal cord neurons using adeno-associated virus vectors containing cell type-specific promoters. Gene Ther. *4*, 16–24.
10. Sohal, V.S., Zhang, F., Yizhar, O., and Deisseroth, K. (2009). Parvalbumin neurons and gamma rhythms enhance cortical circuit performance. Nature *459*, 698–702.
11. Qin, J.Y., Zhang, L., Clift, K.L., Hulur, I., Xiang, A.P., Ren, B.Z., and Lahn, B.T. (2010). Systematic comparison of constitutive promoters and the doxycycline-inducible promoter. PLoS ONE *5*, e10611.
12. Gray, S.J., Foti, S.B., Schwartz, J.W., Bachaboina, L., Taylor-Blake, B., Coleman, J., Ehlers, M.D., Zylka, M.J., McCown, T.J., and Samulski, R.J. (2011). Optimizing promoters for recombinant adeno-associated virus-mediated gene expression in the peripheral and central nervous system using self-complementary vectors. Hum. Gene Ther. *22*, 1143–1153.
13. Jackson, K.L., Dayton, R.D., Deverman, B.E., and Klein, R.L. (2016). Better targeting, better efficiency for wide-scale neuronal transduction with the synapsin promoter and AAV-PHP.B. Front. Mol. Neurosci. *9*, 116.
14. Nathanson, J.L., Jappelli, R., Scheeff, E.D., Manning, G., Obata, K., Brenner, S., and Callaway, E.M. (2009). Short promoters in viral vectors drive selective expression in mammalian inhibitory neurons, but do not restrict activity to specific inhibitory cell-types. Front. Neural Circuits *3*, 19.
15. Brooks, A.R., Harkins, R.N., Wang, P., Qian, H.S., Liu, P., and Rubanyi, G.M. (2004). Transcriptional silencing is associated with extensive methylation of the CMV promoter following adenoviral gene delivery to muscle. J. Gene Med. *6*, 395–404.
16. Bäck, S., Dossat, A., Parkkinen, I., Koivula, P., Airavaara, M., Richie, C.T., Chen, Y.H., Wang, Y., and Harvey, B.K. (2019). Neuronal activation stimulates cytomegalovirus promoter-driven transgene expression. Mol. Ther. Methods Clin. Dev. *14*, 180–188.
17. Husain, T., Passini, M.A., Parente, M.K., Fraser, N.W., and Wolfe, J.H. (2009). Long-term AAV vector gene and protein expression in mouse brain from a small pan-cellular promoter is similar to neural cell promoters. Gene Ther. *16*, 927–932.
18. Powell, S.K., Rivera-Soto, R., and Gray, S.J. (2015). Viral expression cassette elements to enhance transgene target specificity and expression in gene therapy. Discov. Med. *19*, 49–57.
19. Koyuncu, O.O., Hogue, I.B., and Enquist, L.W. (2013). Virus infections in the nervous system. Cell Host Microbe *13*, 379–393.
20. Mangold, C.A., Engel, E.A., Ostler, J.B., Jr., Wilson, A.C., and Cohrs, R.J. (2019). 2019 Colorado Alphaherpesvirus Latency Society symposium. J. Neurovirol. Published online September 9, 2019.
21. Berthomme, H., Lokensgard, J., Yang, L., Margolis, T., and Feldman, L.T. (2000). Evidence for a bidirectional element located downstream from the herpes simplex virus type 1 latency-associated promoter that increases its activity during latency. J. Virol. *74*, 3613–3622.
22. Lokensgard, J.R., Berthomme, H., and Feldman, L.T. (1997). The latency-associated promoter of herpes simplex virus type 1 requires a region downstream of the transcription start site for long-term expression during latency. J. Virol. *71*, 6714–6719.
23. Cheung, A.K. (1989). Detection of pseudorabies virus transcripts in trigeminal ganglia of latently infected swine. J. Virol. *63*, 2908–2913.
24. Priola, S.A., and Stevens, J.G. (1991). The 5′ and 3′ limits of transcription in the pseudorabies virus latency associated transcription unit. Virology *182*, 852–856.
25. Cheung, A.K. (1991). Cloning of the latency gene and the early protein 0 gene of pseudorabies virus. J. Virol. *65*, 5260–5271.
26. Cheung, A.K., and Smith, T.A. (1999). Analysis of the latency-associated transcript/UL1-3.5 gene cluster promoter complex of pseudorabies virus. Arch. Virol. *144*, 381–391.
27. Jin, L., and Scherba, G. (1999). Expression of the pseudorabies virus latency-associated transcript gene during productive infection of cultured cells. J. Virol. *73*, 9781–9788.
28. Jin, L., Schnitzlein, W.M., and Scherba, G. (2000). Identification of the pseudorabies virus promoter required for latency-associated transcript gene expression in the natural host. J. Virol. *74*, 6333–6338.
29. Taharaguchi, S., Kobayashi, T., Yoshino, S., and Ono, E. (2002). Analysis of regulatory functions for the region located upstream from the latency-associated transcript (LAT) promoter of pseudorabies virus in cultured cells. Vet. Microbiol. *85*, 197–208.

30. Ono, E., Tomioka, Y., and Taharaguchi, S. (2007). Possible roles of transcription factors of pseudorabies virus in neuropathogenicity. Fukuoka Igaku Zasshi *98*, 364–372.

31. Deshmane, S.L., and Fraser, N.W. (1989). During latency, herpes simplex virus type 1 DNA is associated with nucleosomes in a chromatin structure. J. Virol. *63*, 943–947.

32. Taharaguchi, S., Yoshino, S., Amagai, K., and Ono, E. (2003). The latency-associated transcript promoter of pseudorabies virus directs neuron-specific expression in trigeminal ganglia of transgenic mice. J. Gen. Virol. *84*, 2015–2022.

33. Fornes, O., Castro-Mondragon, J.A., Khan, A., van der Lee, R., Zhang, X., Richmond, P.A., Modi, B.P., Correard, S., Gheorghe, M., Baranašić, D., et al. (2020). JASPAR 2020: update of the open-access database of transcription factor binding profiles. Nucleic Acids Res. *48* (D1), D87–D92.

34. Nguyen, N.T.T., Contreras-Moreira, B., Castro-Mondragon, J.A., Santana-Garcia, W., Ossio, R., Robles-Espinoza, C.D., Bahin, M., Collombet, S., Vincens, P., Thieffry, D., et al. (2018). RSAT 2018: regulatory sequence analysis tools 20th anniversary. Nucleic Acids Res. *46* (W1), W209–W214.

35. Ziebarth, J.D., Bhattacharya, A., and Cui, Y. (2013). CTCFBSDB 2.0: a database for CTCF-binding sites and genome organization. Nucleic Acids Res. *41*, D188–D194.

36. Wang, J., Pol, S.U., Haberman, A.K., Wang, C., O'Bara, M.A., and Sim, F.J. (2014). Transcription factor induction of human oligodendrocyte progenitor fate and differentiation. Proc. Natl. Acad. Sci. USA *111*, E2885–E2894.

37. Renier, N., Adams, E.L., Kirst, C., Wu, Z., Azevedo, R., Kohl, J., Autry, A.E., Kadiri, L., Umadevi Venkataraju, K., Zhou, Y., et al. (2016). Mapping of brain activity by automated volume analysis of immediate early genes. Cell *165*, 1789–1802.

38. Renier, N., Wu, Z., Simon, D.J., Yang, J., Ariel, P., and Tessier-Lavigne, M. (2014). iDISCO: a simple, rapid method to immunolabel large tissue samples for volume imaging. Cell *159*, 896–910.

39. Chan, L.Y., Mugler, C.F., Heinrich, S., Vallotton, P., and Weis, K. (2018). Non-invasive measurement of mRNA decay reveals translation initiation as the major determinant of mRNA stability. eLife *7*, 7.

40. Deverman, B.E., Ravina, B.M., Bankiewicz, K.S., Paul, S.M., and Sah, D.W.Y. (2018). Gene therapy for neurological disorders: progress and prospects. Nat. Rev. Drug Discov. *17*, 767.

41. Ingusci, S., Verlengia, G., Soukupova, M., Zucchini, S., and Simonato, M. (2019). Gene therapy tools for brain diseases. Front. Pharmacol. *10*, 724.

42. Wang, D., Tai, P.W.L., and Gao, G. (2019). Adeno-associated virus vector as a platform for gene therapy delivery. Nat. Rev. Drug Discov. *18*, 358–378.

43. Chamberlain, K., Riyad, J.M., and Weber, T. (2016). Expressing transgenes that exceed the packaging capacity of adeno-associated virus capsids. Hum. Gene Ther. Methods *27*, 1–12.

44. Colella, P., Sellier, P., Costa Verdera, H., Puzzo, F., van Wittenberghe, L., Guerchet, N., Daniele, N., Gjata, B., Marmier, S., Charles, S., et al. (2018). AAV gene transfer with tandem promoter design prevents anti-transgene immunity and provides persistent efficacy in neonate Pompe mice. Mol. Ther. Methods Clin. Dev. *12*, 85–101.

45. Wang, L., Muramatsu, S., Lu, Y., Ikeguchi, K., Fujimoto, K., Okada, T., Mizukami, H., Hanazono, Y., Kume, A., Urano, F., et al. (2002). Delayed delivery of AAV-GDNF prevents nigral neurodegeneration and promotes functional recovery in a rat model of Parkinson's disease. Gene Ther. *9*, 381–389.

46. Cearley, C.N., and Wolfe, J.H. (2007). A single injection of an adeno-associated virus vector into nuclei with divergent connections results in widespread vector distribution in the brain and global correction of a neurogenetic disease. J. Neurosci. *27*, 9928–9940.

47. Andersson, R., and Sandelin, A. (2020). Determinants of enhancer and promoter activities of regulatory elements. Nat. Rev. Genet. *21*, 71–87.

48. Herdegen, T., and Leah, J.D. (1998). Inducible and constitutive transcription factors in the mammalian nervous system: control of gene expression by Jun, Fos and Krox, and CREB/ATF proteins. Brain Res. Brain Res. Rev. *28*, 370–490.

49. Kriesel, J.D., Jones, B.B., Dahms, K.M., and Spruance, S.L. (2004). STAT1 binds to the herpes simplex virus type 1 latency-associated transcript promoter. J. Neurovirol. *10*, 12–20.

50. Emery, B., and Lu, Q.R. (2015). Transcriptional and epigenetic regulation of oligodendrocyte development and myelination in the central nervous system. Cold Spring Harb. Perspect. Biol. *7*, a020461.

51. Lang, F., Li, X., Vladimirova, O., Hu, B., Chen, G., Xiao, Y., Singh, V., Lu, D., Li, L., Han, H., et al. (2017). CTCF interacts with the lytic HSV-1 genome to promote viral transcription. Sci. Rep. *7*, 39861.

52. Lee, J.S., Raja, P., Pan, D., Pesola, J.M., Coen, D.M., and Knipe, D.M. (2018). CCCTC-binding factor acts as a heterochromatin barrier on herpes simplex viral latent chromatin and contributes to poised latent infection. MBio *9*, e02372-17.

53. Zimmerman, D., Patel, K., Hall, M., and Elmer, J. (2018). Enhancement of transgene expression by nuclear transcription factor Y and CCCTC-binding factor. Biotechnol. Prog. *34*, 1581–1588.

54. Washington, S.D., Musarrat, F., Ertel, M.K., Backes, G.L., and Neumann, D.M. (2018). CTCF binding sites in the herpes simplex virus 1 genome display site-specific CTCF occupation, protein recruitment, and insulator function. J. Virol. *92*, e00156-18.

55. Haberman, R.P., and McCown, T.J. (2002). Regulation of gene expression in adeno-associated virus vectors in the brain. Methods *28*, 219–226.

56. Kenny, J.J., Krebs, F.C., Hartle, H.T., Gartner, A.E., Chatton, B., Leiden, J.M., Hoeffler, J.P., Weber, P.C., and Wigdahl, B. (1994). Identification of a second ATF/CREB-like element in the herpes simplex virus type 1 (HSV-1) latency-associated transcript (LAT) promoter. Virology *200*, 220–235.

57. Leib, D.A., Nadeau, K.C., Rundle, S.A., and Schaffer, P.A. (1991). The promoter of the latency-associated transcripts of herpes simplex virus type 1 contains a functional cAMP-response element: role of the latency-associated transcripts and cAMP in reactivation of viral latency. Proc. Natl. Acad. Sci. USA *88*, 48–52.

58. Baskerville, A., and Lloyd, G. (1977). Experimental infection of monkeys with *Herpesvirus suis* (Aujeszky's-disease virus). J. Med. Microbiol. *10*, 139–144.

59. Wong, G., Lu, J., Zhang, W., and Gao, G.F. (2019). Pseudorabies virus: a neglected zoonotic pathogen in humans? Emerg. Microbes Infect. *8*, 150–154.

60. Rincon, M.Y., de Vin, F., Duqué, S.I., Fripont, S., Castaldo, S.A., Bouhuijzen-Wenger, J., and Holt, M.G. (2018). Widespread transduction of astrocytes and neurons in the mouse central nervous system after systemic delivery of a self-complementary AAV-PHP.B vector. Gene Ther. *25*, 83–92.

61. McCarty, D.M. (2008). Self-complementary AAV vectors; advances and applications. Mol. Ther. *16*, 1648–1656.

62. Patrício, M.I., Barnard, A.R., Orlans, H.O., McClements, M.E., and MacLaren, R.E. (2017). Inclusion of the woodchuck hepatitis virus posttranscriptional regulatory element enhances AAV2-Driven transduction of mouse and human retina. Mol. Ther. Nucleic Acids *6*, 198–208.

63. Fagoe, N.D., Eggers, R., Verhaagen, J., and Mason, M.R. (2014). A compact dual promoter adeno-associated viral vector for efficient delivery of two genes to dorsal root ganglion neurons. Gene Ther. *21*, 242–252.

64. Ramezani, A., Hawley, T.S., and Hawley, R.G. (2000). Lentiviral vectors for enhanced gene expression in human hematopoietic cells. Mol. Ther. *2*, 458–469.

65. Paterna, J.C., Moccetti, T., Mura, A., Feldon, J., and Büeler, H. (2000). Influence of promoter and WHV post-transcriptional regulatory element on AAV-mediated transgene expression in the rat brain. Gene Ther. *7*, 1304–1311.

66. Xia, X., Zhang, Y., Zieth, C.R., and Zhang, S.C. (2007). Transgenes delivered by lentiviral vector are suppressed in human embryonic stem cells in a promoter-dependent manner. Stem Cells Dev. *16*, 167–176.

67. Choi, J.H., Yu, N.K., Baek, G.C., Bakes, J., Seo, D., Nam, H.J., Baek, S.H., Lim, C.S., Lee, Y.S., and Kaang, B.K. (2014). Optimization of AAV expression cassettes to improve packaging capacity and transgene expression in neurons. Mol. Brain *7*, 17.

68. Zolotukhin, S., Byrne, B.J., Mason, E., Zolotukhin, I., Potter, M., Chesnut, K., Summerford, C., Samulski, R.J., and Muzyczka, N. (1999). Recombinant adeno-associated virus purification using novel methods improves infectious titer and yield. Gene Ther. *6*, 973–985.

69. Curanovic, D., Ch'ng, T.H., Szpara, M., and Enquist, L. (2009). Compartmented neuron cultures for directional infection by alpha herpesviruses. Curr. Protoc. Cell Biol. *Chapter 26*. Unit 26.4.

70. Yardeni, T., Eckhaus, M., Morris, H.D., Huizing, M., and Hoogstraten-Miller, S. (2011). Retro-orbital injections in mice. Lab Anim. (NY) *40*, 155–160.

71. Maturana, C.J., Aguirre, A., and Sáez, J.C. (2017). High glucocorticoid levels during gestation activate the inflammasome in hippocampal oligodendrocytes of the offspring. Dev. Neurobiol. *77*, 625–642.